Mitochondrial Respiration, Cardiac Function and Hemodynamics in Rats on High-Calorie Diets with Metabolic Syndrome and Diabetes

Evgenii Ivanov *, Marina Akhmetshina , Aleksei Erdiakov , Albina Gizatulina , Svetlana Gavrilova

Posted Date: 10 November 2023

doi: 10.20944/preprints202311.0720.v1

Keywords: diabetes mellitus; metabolic syndrome; obesity; adipose tissue; OXPHOS; mitochonrdial respiration

Article

Mitochondrial Respiration, Cardiac Function and Hemodynamics in Rats on High-Calorie Diets with Metabolic Syndrome and Diabetes

Evgenii Ivanov *, Marina Akhmetshina, Aleksei Erdiakov, Albina Gizatulina and Svetlana Gavrilova

Faculty of Medicine, Lomonosov Moscow State University, Moscow 119991, Russia; akhmetshinamr@yandex.ru (M.A.); hemiun@mail.ru (A.E.); albina.giz@yandex.ru (A.G.); sgavrilova@mail.ru (S.G.)

* Correspondence: ivanovev102@yandex.ru

Abstract: In a 24-week-long experiment, 31 rats were assigned to one of 3groups: a Control group receiving standard chow and water, a Fructose group receiving standard chow and a 20% fructose solution, or an STZ+lipids group that received a fat-enriched diet following a single 25 mg/kg streptozotocin injection at the onset of the diet. The STZ+lipids group exhibited hyperglycemia, hyperketonemia, and a decline in both heart rate and cardiac function. Conversely, there were no significant biochemical differences between the Fructose and Control groups. However, the Fructose group experienced a more pronounced decrease in heart function. Respirometric analyses unveiled a substantial increase in mitochondrial respiration across all adipose tissue types in both dietary intervention groups, with greater changes observed in the Fructose group. Correlation analyses demonstrated a positive association between respiratory indices and fat volume, heart function, and tissue blood flow in the Control group. In the STZ+lipids and Fructose groups, respiratory indices exhibited a positive correlation with heart rate and a negative correlation with dietary exposure characteristics. Overall, the markedly elevated mitochondrial respiration rate observed in rats subjected to hypercaloric diets was linked to characteristics indicative of dietary resilience, rather than measures of circulation.

Keywords: diabetes mellitus; metabolic syndrome; obesity; adipose tissue; mitochondrial respiration; OXPHOS

1. Introduction

Metabolic syndrome (MetS) is a complex of interconnected metabolic, regulatory, and neuroendocrine abnormalities that culminate in the development of visceral obesity, hyperglycemia, and insulin resistance (IR). Given the pervasive prevalence of sedentary lifestyle unhealthy dietary habits characterized by the excessive consumption of processed foods laden with excess fat and carbohydrates, and a genetic predisposition, MetS has emerged as a burgeoning global health concern, affecting an increasingly large segment of the population. Individuals afflicted with MetS face a significantly elevated risk of developing type 2 diabetes mellitus, cardiovascular pathologies such as heart failure, arrhythmias, coronary and peripheral arterial complications, and stroke [1–4].

In cases of severe type 2 diabetes, morbid obesity, and other profound pathological states, researchers have documented a substantial decline in mitochondrial function through numerous investigations. This mitochondrial dysfunction is linked to insulin resistance, ectopic lipid accumulation, abnormal apoptosis, and noticeable functional impairment across various organs. Prominent factors contributing to mitochondrial dysregulation and damage include the accumulation of reactive oxygen species, impairment of DNA repair, increase in production of toxic metabolic intermediates, protein glycosylation, and the activation of many other pathological pathways [5,6]. Nevertheless, as individuals progress through the continuum of diabetes, MetS, and its complications, mitochondria may undergo diverse functional rearrangements that remain poorly

Preprints (www.preprints.org) | NOT PEER-REVIEWED | Posted: 10 November 2023 doi:10.20944/preprints202311.0720.v1

understood. While severe complications of MetS typically correspond to decreased oxidative phosphorylation (OXPHOS), studies conducted on mild obesity-related pathologies and experimental models have unveiled a spectrum of changes ranging from moderate impairment to a sufficient respiration increase. Furthermore, these changes exhibit regional disparities in various tissues. Special attention has been directed towards adipose tissues, as numerous studies have highlighted the pivotal role of impaired lipid storage in the development of MetS. However, due to the heterogeneous nature of models and methodologies employed, conflicting reports abound regarding tissue respiration in different organs. Respiratory function in liver and muscles, for instance, has been observed to vary from a moderate decline to a moderate enhancement [7,8]. It is worth noting that some research has suggested that mitochondrial stimulation leading to increased bioenergetics can ameliorate obesity-related disorders in certain MetS models [9,10].

In the scope of our study, we decided to investigate two distinct models of obesity-related disorders: a MetS rat model induced by the replacement of water with a 20% fructose solution, representing a less complicated MetS model, and a type 2 diabetes rat model induced by a lipid-enriched diet combined with a single 25 mg/kg streptozotocin injection, replicating severe impairment. Typically, fructose-enriched diets do not result in a significant weight gain but do shift lipid storage towards visceral adipose tissues. Conversely, lipid-enriched diet models combined with streptozotocin injections can induce severe hyperglycemia and other metabolic disturbances, including weight gain and dyslipidemia. In our study, we placed particular emphasis on examining characteristics of the cardiovascular system, because blood flow in peripheral tissues exerts a profound influence on metabolic processes, and a complex interplay between circulation and adipose tissue metabolism exists.

2. Results

2.1. Metabolic syndrome features

By the end of the study, all rats exhibited a notable increase in body weight. Although no statistically significant differences were observed among the groups, there was a noticeably greater dispersion in body weight within the experimental diet groups, with the STZ+lipids group showing the most evident variability (Figure 1A). Food consumption throughout the study exhibited significant variations across all three groups. Specifically, rats in the Fructose group consumed considerably less food while receiving an equivalent calorie intake to the STZ+lipids group rats. Caloric intake was significantly higher in both experimental groups compared to the Control group. Furthermore, water intake was significantly elevated in both the STZ+lipids and Fructose groups when compared to the Control group (Table 1).

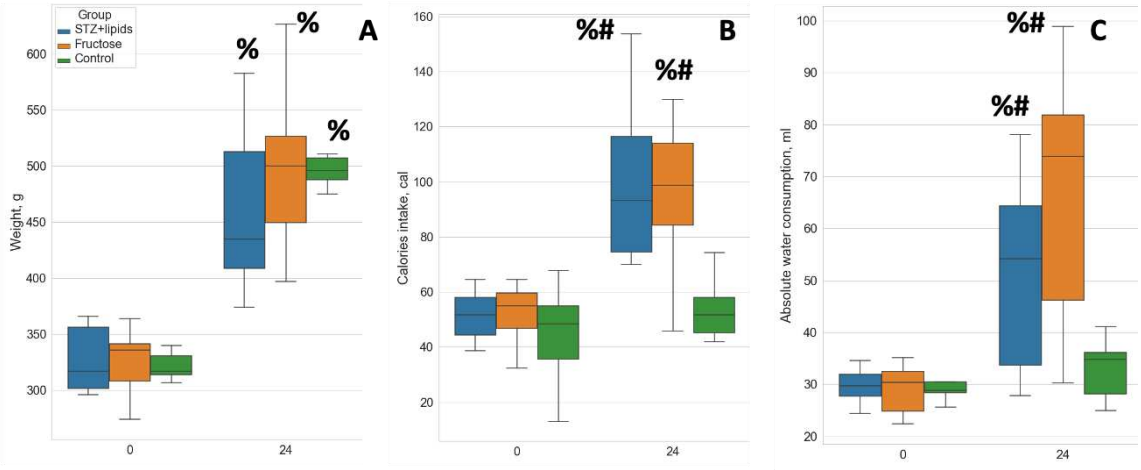

Figure 1. Boxplot of metabolic feature values. A – weight, B – calorie intake, C – absolute water consumption. # - p<0.05 compared to control, % - p<0.05 comparing week 0 and week 24.

Preprints (www.preprints.org) | NOT PEER-REVIEWED | Posted: 10 November 2023 doi:10.20944/preprints202311.0720.v1

Table 1. Major metabolic features in 3 groups at the beginning (week 0) and at the end (week 24) of the experiment. Data presented as median (IQR).

	Control		STZ+lipids		Fructose	
Week	0	24	0	24	0	24
Weight, g	317.00(314.00, 331.00)	496.00(483.50, 508.50)	317.00(302.00, 356.50)	435.00(409.00, 513.00)	336.00(308.50, 341.50)	500.00(449.50, 527.00)
Total energy intake, cal/day	48.39(35.49, 54.84)	51.62(45.16, 58.07)	51.62(46.78, 58.07)	93.19(74.55, 116.49)	54.84(46.78, 59.68)	98.61(84.30, 113.90)
Water consumption, ml/day	28.84(28.35, 30.48)	34.76(28.11, 36.16)	29.75(27.71, 31.93)	54.19(33.70, 64.37)	30.41(24.80, 32.50)	73.88(46.16, 81.82)
Glucose, mmol/l	6.20(6.10, 6.50)	6.15(5.85, 6.55)	5.90(5.70, 6.45)	20.90(14.00, 21.90)	6.00(5.60, 6.20)	6.40(6.30, 6.65)
Ketone bodies, mmol/l	0.90(0.80, 0.90)	0.80(0.70, 0.80)	0.90(0.80, 1.00)	1.00(0.85, 1.65)	1.00(0.95, 1.00)	0.80(0.65, 0.85)
Triglycerides, mmol/l	0.41(0.38, 0.62)	0.62(0.50, 1.14)	0.55(0.38, 0.66)	1.43(0.73, 1.52)	0.37(0.33, 0.46)	0.84(0.63, 1.15)
Insulin, microU/l	8.29(5.82, 16.51)	2.02(1.70, 2.48)	5.53(2.37, 11.05)	1.47(0.93, 1.88)	4.21(2.80, 5.47)	2.42(1.62, 3.83)
HOMA-IR	3.12(2.62, 6.38)	1.33(1.04, 1.82)	2.14(0.88, 4.00)	1.52(0.70, 2.26)	1.41(0.66, 2.12)	1.28(0.98, 2.31)

The injection of streptozotocin induced a marked and sustained elevation in glucose levels. After 24 weeks of the experiment, glucose level was significantly higher in the STZ+lipids group when compared to both the Fructose and Control groups, with a median level of 21 mmol/l (Figure 2A, $p<0.01$). Additionally, rats in the STZ+lipids group exhibited a significant increase in ketone bodies, with levels significantly higher than those in both the Fructose and Control groups, with a median level of approximately 1 mmol/l (Figure 1D). Notably, insulin levels exhibited a significant reduction in the blood of rats in both the STZ+lipids and Control groups, with no significant differences observed between these two groups (Figure 2B).

Based on insulin and glucose levels, the HOMA-IR index was found to be consistent across all groups at week 24, providing no evidence for insulin resistance (Figure 2C). Dyslipidemia features were assessed by measuring venous blood triglyceride levels. Surprisingly, a significant increase was observed in all three groups, including the Control group. Triglyceride levels tended to be higher in the STZ+lipids group when compared to the Control group ($p=0.068$) and the Fructose group ($p=0.09$) (Figure 2E). Interestingly, the TyG surrogate insulin resistance index was significantly elevated in the STZ+lipids group (Figure 2E), although we did not conduct gold standard tests for comparing insulin resistance.

The impact of weight gain varied among the three groups and was influenced by various factors. In the Control group, weight exhibited a maximal positive correlation with food consumption ($R=0.46$) and a maximal negative correlation with water intake ($R = -0.48$). Notably, while glucose concentration remained within the normal range, it displayed a significant negative correlation with cholesterol levels ($R=-0.75$) and triglyceride concentration ($R=-0.49$, see Suppl. 1A).

In the Fructose group, weight was significantly correlated with calorie intake ($R=0.74$), particularly with the consumption of carbohydrates ($R=0.71$). This weight gain was associated with higher triglyceride concentration ($R=0.92$) and insulin concentration ($R=0.65$), but not with glucose concentration ($R=-0.37$, see Suppl. 1B).

Preprints (www.preprints.org) | NOT PEER-REVIEWED | Posted: 10 November 2023 doi:10.20944/preprints202311.0720.v1

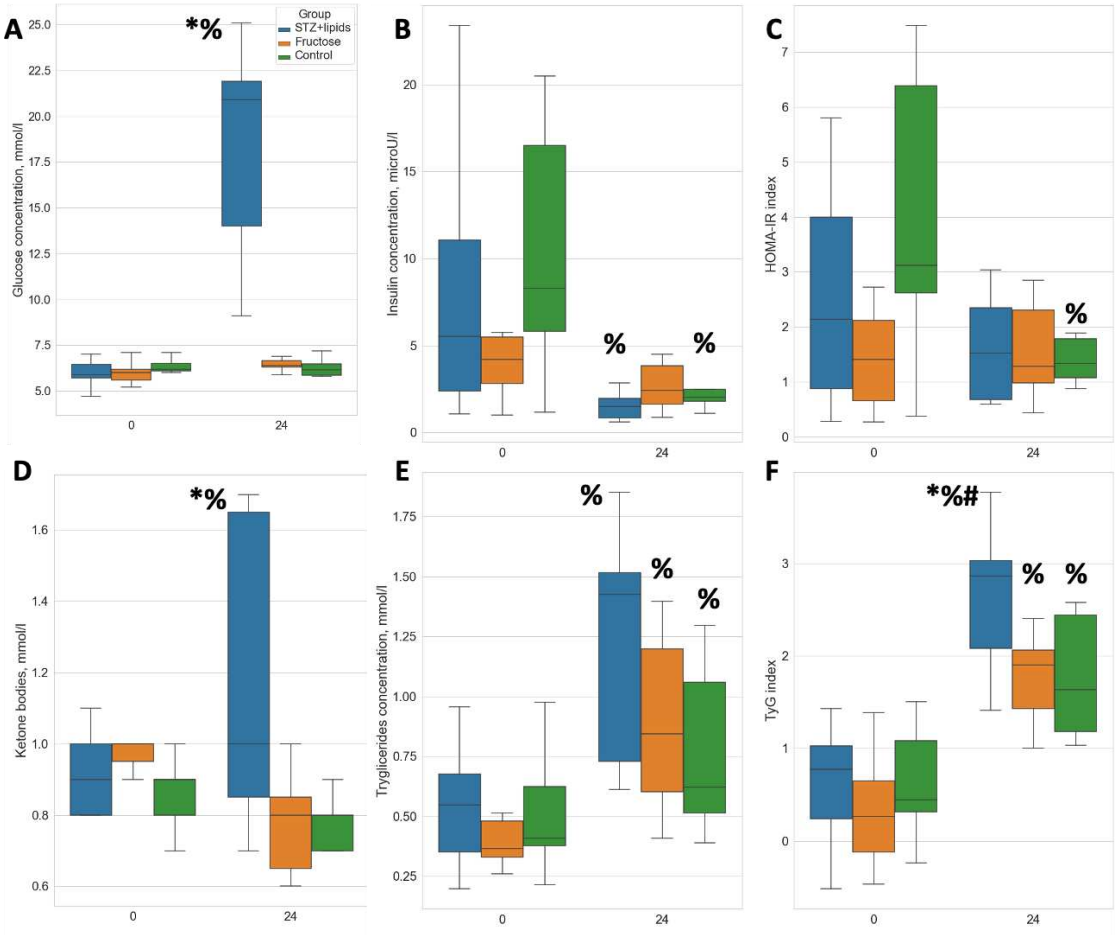

Figure 2. Boxplot of biochemical feature values. A – glucose concentration, B – insulin concentration, C – HOMA-IR index values, D – ketone bodies concentration, E – triglycerides concentration, F – TyG index values. # - p<0.05 compared to control, * - p<0.05 comparing the STZ+lipids and Fructose groups, % - p<0.05 comparing week 0 and week 24.

In contrast, the STZ+lipids group presented a different pattern, with higher weight observed in rats with less severe metabolic disturbances. Weight exhibited negative correlations with ketone bodies concentration (R=-0.61) and glucose concentration (R=-0.46), but no correlation with food consumption (R=0.18). However, the biochemical changes in this group aligned with an increase in food consumption, showing significant correlations with ketone bodies concentration (R=0.77), triglyceride concentration (R=0.76), and to a lesser extent, glucose concentration (R=0.5) and cholesterol concentration (R=0.42, see Suppl. 1C).

We assessed adipose tissue depots using an ultrasound probe both at the baseline and at the end of the experiment. As simplified markers of depot volume, we measured the maximal thickness or area of three distinct depots. Subcutaneous adipose tissue (SAT) was assessed in the inguinal region, along the femoral bone. Brown adipose tissue (BAT) was evaluated in the subscapular pads, while visceral adipose tissue (VAT) was quantified as the maximal transverse area of perirenal adipose tissue.

Interestingly, there was a tendency for visceral fat area to increase in all groups, although statistically significant changes were only observed in the STZ+lipids group, where it increased from 0.61 ± 0.12 cm^2 to 0.84 ± 0.3 cm^2 (p=0.028). Simultaneously, the mean subcutaneous fat thickness decreased in all groups with significant changes noted in both the STZ+lipids (1.8 ± 0.24 mm to 1.46 ± 0.33 mm, p=0.01) and the Control group (1.64 ± 0.29 mm to 1.26 ± 0.6 mm, p=0.035).

Furthermore, the brown fat area increased up to the 24th week with significant changes observed in the STZ+lipids and Fructose groups. The subscapular fat area also saw an increase in the STZ+lipids group, rising from 0.7 ± 0.04 cm^2 to 0.8 ± 0.09 cm^2 (p=0.024), and in the Fructose group,

Preprints (www.preprints.org) | NOT PEER-REVIEWED | Posted: 10 November 2023 doi:10.20944/preprints202311.0720.v1

increasing from 0.62 ± 0.09 cm² to 0.71 ± 0.13 cm² (p=0.035). Importantly, there were no significant differences observed between the groups in independent tests. Finally, subscapular adipose tissue was weighed at the end of the experiment, but no significant differences between the groups were found.

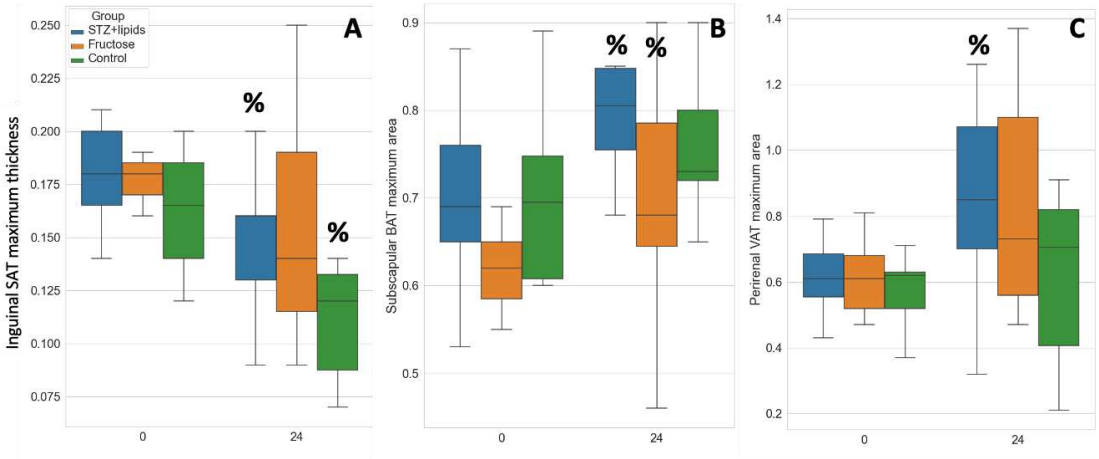

Figure 3. Boxplot of adipose tissues ultrasound evaluation results. A – subcutaneous adipose tissue, B – brown adipose tissue, C – visceral adipose tissue. % - p<0.05 comparing week 0 and week 24.

2.2. Hemodinamic features

As we did not observe higher rates of metabolic disturbances, we also did not anticipate the emergence of severe ischemic complications. The STZ+lipids group exhibited persistent and severe hyperglycemia, which could potentially lead to endothelial damage to some extent. Some studies have also linked this type 2 diabetes model to arterial hypertension and cardiomyopathies. In different circumstances, the metabolic syndrome model appears to manifest varying degrees of circulatory issues. In our study, we comprehensively evaluated local and systemic conditions of the cardiovascular system. We conducted non-invasive measurements of arterial pressure, including systolic blood pressure (sBP), diastolic blood pressure (dBP), and pulse blood pressure (pulse BP). These parameters did not exhibit significant differences at month 4, either between the groups or when compared to baseline measurements (Figure 4 A, B), with the exception of the Control group's pulse pressure (Figure 4 C, D), which significantly decreased compared to both the STZ+lipids group and the baseline measurements.

A significantly altered overall state of the cardiovascular system was evident in the STZ+lipids group, marked by a notable decrease in heart rate (HR). HR was measured in awake animals concurrently with BP measurements and initially ranged from 377 to 394 bpm without significant differences. However, by month 4, the heart rate in STZ+lipids rats had declined to 316 bpm, with a p-value of less than 0.05 when compared to all other groups at each time point. This bradycardia could potentially be attributed to either the impact of severe hyperglycemia on the heart's pacemaker or disturbances in the autonomic nervous system.

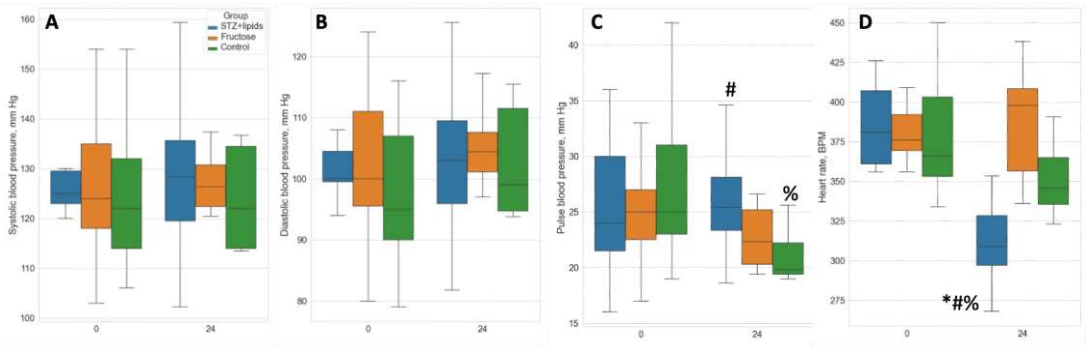

 doi:10.20944/preprints202311.0720.v1

Figure 4. Boxplot of blood pressure and heart rate values. A – systolic blood pressure, B – diastolic blood pressure, C – pulse blood pressure, D – heart rate. # - $p<0.05$ compared to Control group, * - $p<0.05$ comparing the STZ+lipids and Fructose groups, % - $p<0.05$ comparing week 0 and week 24.

Interestingly, we observed severe heart pumping function failure after 6 months of the experimental diet in both metabolic syndrome and diabetes groups compared to the Control group. While the mean ejection fraction (EF) at baseline ranged from 72.8% to 75.5%, by the 6-month mark, it had decreased to 68.2% ± 4.6% in the Control group ($p=0.007$ compared to baseline). In the STZ+lipids group, EF dropped to 55.6% ± 5.7% ($p<0.001$ compared to control), and in the Fructose group, it decreased to 54.2% ± 11.1% ($p=0.004$ compared to control) (Figure 5C). The decrease in EF in both experimental groups was statistically significant compared to baseline ($p<0.001$). Stroke volume remained relatively stable in all three groups, with no significant changes compared to baseline, but intergroup differences were observed between the experimental and Control groups (Figure 5D).

End-systolic volume (ESV) showed a dramatic increase in both experimental groups, indicative of systolic dysfunction. While ESV also increased significantly in the Control group, it exhibited a tendency to be lower than that in the experimental groups. Anyway, heart failure features did not lead to decline in the tissue blood flow, indicating it did not have a clinical importance. We did not find any statistically significant changes in the LDF values in any group.

Preprints (www.preprints.org) | NOT PEER-REVIEWED | Posted: 10 November 2023 doi:10.20944/preprints202311.0720.v1

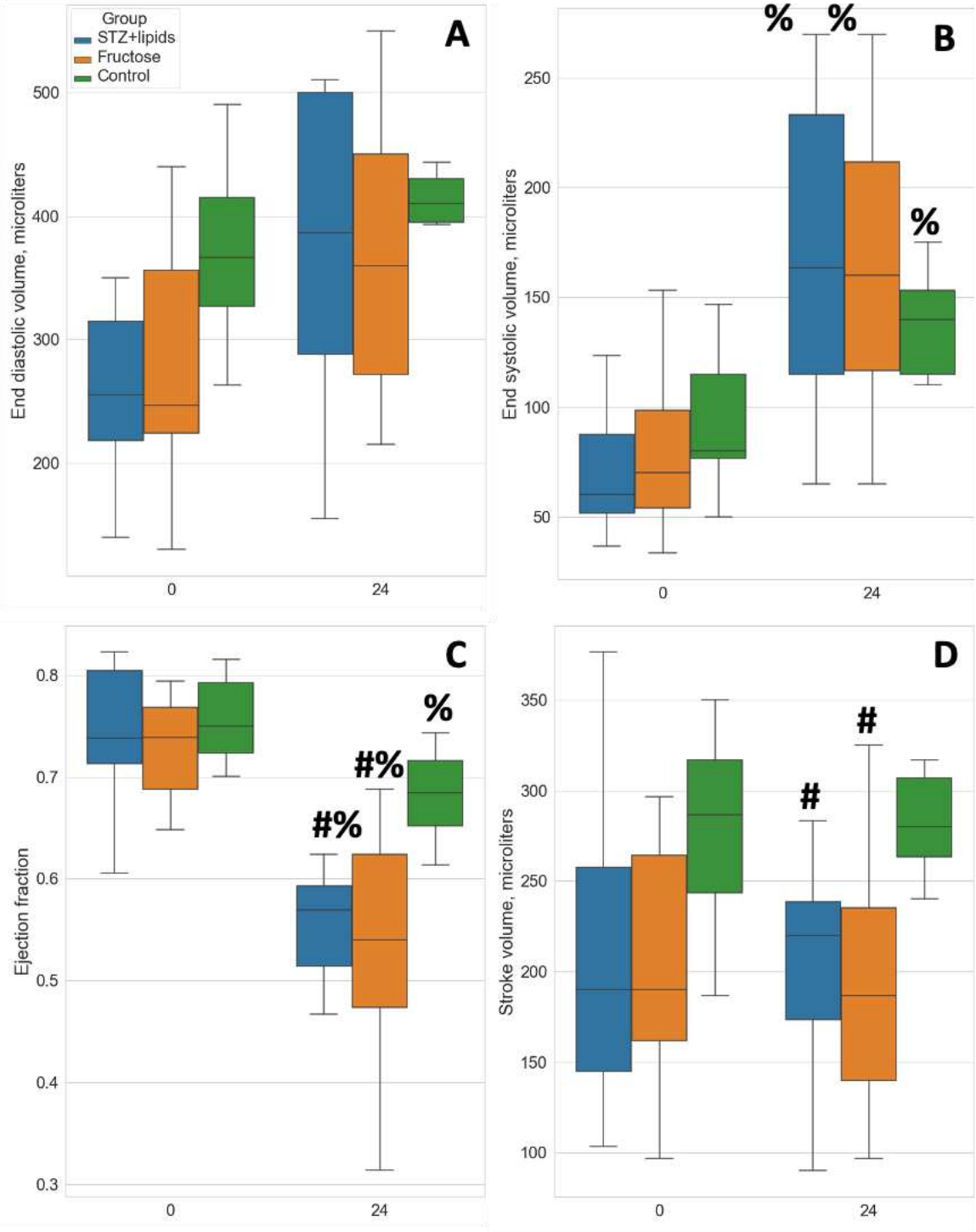

Figure 5. Boxplot of heart function values. A – end diastolic volume, B – end systolic volume, C – ejection fraction, D – stroke volume. # - $p<0.05$ compared to Control, % - $p<0.05$ comparing week 0 and week 24.

Overall tissue circulation was accessed by laser doppler flowmetry (LDF). We calculated mean value in arbitrary tissue perfusion units (PFU) in the soft tissues of the back. We did not find any significant differences neither between groups, nor between the baseline and the end-point.

To unravel the underlying causes of hemodynamic alterations, we conducted an analysis of correlations between circulatory parameters and metabolic characteristics. Within the Control group, we observed that higher body weight exhibited significant positive associations with several

 doi:10.20944/preprints202311.0720.v1

hemodynamic variables, including pulse blood pressure (R=0.75), mean tissue blood flow (R=0.67), and stroke volume (R=0.62). Conversely, caloric intake displayed distinct correlations with other hemodynamic parameters, specifically systolic blood pressure (sBP) (R=0.77), diastolic blood pressure (dBP) (R=0.75), and ejection fraction (R=0.54) (see Supplementary Figure 2A).

In contrast, within the Fructose group, most of the previously observed correlations between hemodynamics and metabolic features were dissipated. Only heart rate maintained a significant correlation, notably with glucose concentration (R=0.75) and, to a lesser extent, with caloric intake (R=0.42) (see Supplementary Figure 2B).

In the STZ+lipids group, caloric intake demonstrated noteworthy associations with several hemodynamic parameters, including end-diastolic volume (EDV) (R=0.61), stroke volume (R=0.59), and end-systolic volume (ESV) (R=0.57). On the other hand, glucose concentration exhibited inverse correlations with diastolic blood pressure (dBP) (R=-0.64), systolic blood pressure (sBP) (R=-0.61), stroke volume (R=0.57), and heart rate (R=-0.55) (see Supplementary Figure 2C)."

2.3. Respirometry analysis

Solid tissue samples exhibit significant variability in structure, and the oxygen consumption rate (OCR) is profoundly influenced by the architectural features of the organ. The advancement of intact tissue respirometry encompasses several benefits, including sustained tissue viability, reduced time from excision to testing, preservation of cellular properties, and expedited preparation. Furthermore, we postulate that the architectural integrity of intact tissue samples mitigates the spillage of cytoplasmic components following permeabilization. This phenomenon may elucidate certain deviations from the anticipated OCR dynamics observed during the SUIT protocol. Although the enhanced dynamics enable a reduction in testing time, they do come at the cost of decreased parameter stability. Therefore, we regard this modification of respirometry as a rapid screening approach for identifying more prominent effects and relationships.

Permeabilization with saponin promptly resulted in a significant increase in respiration rate across all tissue types. However, OCR subsequently declined in state 2, and further ADP injection led to an increase in OCR via complex I. Interestingly, the addition of succinate to stimulate complex I+II respiration did not elicit a substantial increase in OCR in any of the tissues studied. We hypothesize that complex II was already sufficiently saturated in the tissue samples under investigation. Notably, even nanogram/ml doses of oligomycin efficiently induced a leak respiration state with low OCR values. The subsequent SUIT step typically involves protonophore titration. In some instances, we observed consistent OCR rates after multiple CCCP injections across different tissue samples. To expedite testing, we administered the same single CCCP dose to all tissues. Overall, the maximal electron transport system (ETS) flow was several times higher than the leak OCR but approximated the rate of state 3 respiration. This pattern aligns with observations reported by some authors, which they attribute to a high degree of permeabilization.

To evaluate complex II respiration, we employed rotenone to inhibit electron flow from complex I, revealing the rate of complex II-mediated respiration. Notably, the OCR attributed to complex II was markedly lower in comparison to that of complex I or ETS. In the control group, complex II OCR was nearly negligible in all adipose tissues. Finally, we treated the samples with the complex III inhibitor Antimycin A to uncover residual respiration, which was subsequently subtracted from all OCR values. The residual respiration rate was negligible across all adipose tissues.

In our investigation utilizing OCR studies were conducted on isolated tissues, we observed a discernible trend of elevated respiration rates in the high-energy diet groups, although it is important to note that the statistical significance of these findings was limited due to the small sample size and considerable data spread. To assess group differences, we employed Kruskal-Wallis tests followed by DSCF post-hoc tests. While the median values indicated higher respiration rates in nearly all respiratory states across the three adipose tissues, the most notable and statistically significant differences were observed within the visceral adipose tissue.

Specifically, in the Fructose group, OCR rates were consistently higher compared to the Control group across various respiration states, including intact respiration, complex I state 3 respiration,

Preprints (www.preprints.org) | NOT PEER-REVIEWED | Posted: 10 November 2023 doi:10.20944/preprints202311.0720.v1

LEAK, ETS, and CII respiration. Conversely, in the STZ+lipids group, OCR rates displayed a trend towards significant differences compared to the Control group in multiple respiration states, with significance reaching statistical significance only in the case of CII respiration within the visceral adipose tissue. In the subcutaneous adipose tissue, the Fructose group exhibited higher OCR rates in the permeabilized state when compared to the Control group. Furthermore, in the brown adipose tissue, the Fructose group demonstrated elevated OCR rates in various respiratory states, including intact, permeabilized, CI, and CI+CII respiration, when compared to the Control group.

Table 2. OCR values in 3 types of adipose tissues. Data presented as median (IQR) in pmol/s/ml/mg.

	Brown adipose tissue			**Subcutaneous adipose tissue**			**Visceral adipose tissue**		
Respiration state	STZ+lipids	Fructose	Control	STZ+lipids	Fructose	Control	STZ+lipids	Fructose	Control
Intact	3.3 (1.7,4.5)	4.0 (3.7,4.8)	2.1 (1.7,2.3)	2.4 (1.2,5.1)	2.4 (1.3,4.9)	1.5 (1.3,2.0)	1.7 (1.3,2.4)	1.7 (1.5,2.1)	1.1 (0.9,1.15)
Permeabilized	3.1 (2.4,6.0)	3.6 (3.0,4.2)	2.0 (1.8,2.2)	2.7 (2.0,3.3)	2.1 (1.2,5.0)	1.3 (1.2,1.7)	1.9 (1.35,2.4)	1.6 (1.4,3.7)	1.15 (1.0,1.4)
Complex I	2.5 (1.5,4.1)	3.8 (2.9,4.7)	1.9 (1.3,2.2)	1.8 (1.1,2.0)	2.4 (1.5,7.2)	1.2 (0.9,1.5)	1.1 (0.8,1.75)	1.6 (1.4,2.3)	0.7 (0.6,0.8)
Complex I+II	3 (2.3,4.0)	3.1 (2.9,4.7)	1.8 (1.5,2.1)	1.8 (0.9,3.1)	1.4 (1.1,6.5)	1.0 (0.7,1.2)	1.3 (0.8,1.7)	1.4 (1.2,2.1)	0.7 (0.5,0.75)
LEAK	0.01 (0,0.9)	0.5 (0.1,1.7)	0.8 (0.05,0.9)	0.1 (0,1.0)	0.3 (0.1,0.5)	0.2 (0.05,0.4)	0.04 (0.01,0.7)	0.3 (0.1,0.5)	0.01 (0,0.07)
Maximal ETS	3.1 (1.8,5.1)	3.2 (2.5,5.0)	1.8 (1.7,2.0)	1.5 (0.9,2.2)	2.3 (1.1,3.7)	0.9 (0.8,1.4)	1.5 (0.8,1.8)	1.8 (1.3,2.0)	0.6 (0.5,0.7)
CII respiration	0.6 (0,1.3)	0.4 (0,1.7)	0.01 (0,0.15)	0.01 (0,0.2)	0.01 (0,0.05)	0.01 (0,0.15)	0.1 (0,0.3)	0.14 (0.01,0.4)	0.01 (0,0.02)

In summary, high-energy diets appear to elicit a substantial increase in mitochondrial respiration. The Fructose metabolic syndrome model offers a continuous influx of readily available nutrients, primarily impacting insulin-dependent tissues. Conversely, the STZ+lipids diabetes model results in reduced insulin levels, potentially leading to diminished nutrient delivery to adipose tissue and a consequent reduction in respiratory capacity. Remarkably, in both models, rats did not exhibit greater weight gain compared to the Control group, despite a significantly higher caloric intake sustained over the course of the 24-week experiment. This suggests that the heightened adipose tissue respiration observed may signify an acquired ability of fat tissue to efficiently utilize excessive nutrients, potentially through an increase in mitochondrial abundance or an upregulation of oxidative phosphorylation (OXPHOS). It is prudent to delve deeper into exploring the temporal dynamics of oxygen consumption rate (OCR) alterations and the underlying mechanisms governing mitochondrial regulation in order to gain further insights.

Preprints (www.preprints.org) | NOT PEER-REVIEWED | Posted: 10 November 2023 doi:10.20944/preprints202311.0720.v1

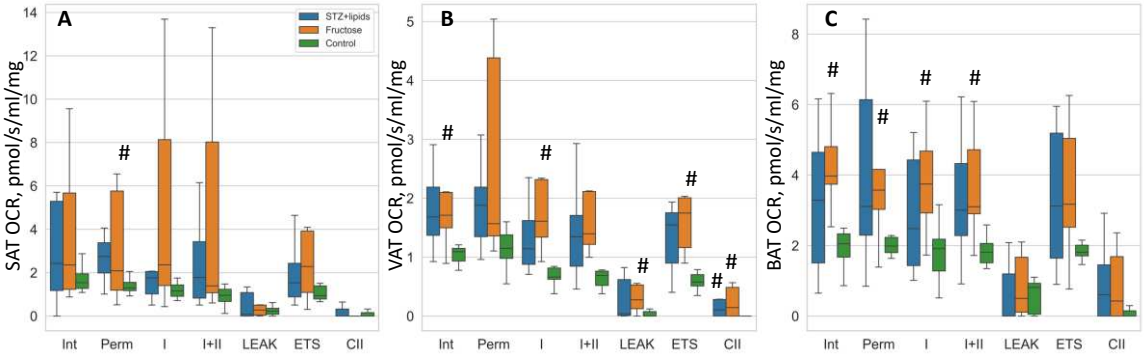

Figure 6. Boxplot of mitochondrial respiration rates. A – SAT, B – VAT, C – BAT. # - p<0.05 compared to the Control. Int – intact respiration, Perm – permeabilized respiration, I – complex I respiration, I+II – complex I + complex II respiration, LEAK – uncoupled respiration, ETS – maximal electron transport system respiration, CII – isolated complex II respiration.

Correlation analyses have revealed a positive association between respiratory indexes and fat volume, heart function, and tissue blood flow in the Control group. In both the STZ+ lipids group and the Fructose group, respiratory indexes exhibited a positive correlation with heart rate and a negative correlation with diet exposure characteristics. Overall, the significantly elevated mitochondrial respiration observed in rats exposed to hypercaloric diets was found to be linked to their ability to withstand dietary challenges, rather than being associated with measures of circulation.

Table 3. Correlations for OCR value in different groups, different adipose depots.

Control	R	p	STZ+lipids	R	p	Fructose	R	p
SAT			**SAT**			**SAT**		
End diastolic volume	0,69	0,060	Heart rate	0,57	0,082	Triglycerides concentration	-0,68	0,043
Stroke volume	0,68	0,061				TyG index	-0,67	0,048
Mean LDF	0,63	0,093				Body weight	-0,55	0,097
VAT						**VAT**		
Mean LDF	0,77	0,041				TyG index	-0,72	0,018
End diastolic volume	0,75	0,053				Triglycerides concentration	-0,68	0,029
End systolic volume	0,68	0,089				Pure water consumption	-0,55	0,099
VAT			**BAT**			**BAT**		
Glucose concentration	0,68	0,092	Food consumption	-0,57	0,088	Glucose concentration	0,80	0,010
Pure water consumption	-0,67	0,097				BAT weight	-0,74	0,037
VAT area	0,67	0,100				Heart rate	0,69	0,038

3. Discussion

Cellular respiration is a complex process influenced by multiple factors, including mitochondrial density, substrate availability, regulatory modifications, ROS (Reactive Oxygen Species) production, mitochondrial membrane composition, and more. Obesity and obesity-related conditions stem from an abundance of low-quality energetic substrates. Key biochemical changes occur within adipose depots, where additional substrates are stored and managed. Most lipids are stored in subcutaneous adipose tissue (SAT) depots, but their overload redirects nutrient flow to visceral adipose tissue (VAT), contributing to more severe obesity and Metabolic Syndrome (MetS). Brown and beige adipocytes are notable for their ability to uncouple Oxidative Phosphorylation (OXPHOS) through the specific UCP1 protein, directly converting energetic metabolites into heat. However, these

 doi:10.20944/preprints202311.0720.v1

adipocytes are not abundant in adults, and limited data exist regarding OXPHOS activity in adipocytes during MetS development.

In our study, we assessed cellular respiration in permeabilized adipose tissue samples from three groups of male Wistar rats: the Control group, being fed a standard chow diet; the Fructose group, which received a 20% fructose solution instead of water; and the STZ+lipids group, that were administrated a lipid-enriched diet and a single 25 mg/kg streptozotocin injection. We followed the standard SUIT protocol for assessing tissue respiration [11]. Generally, all respiratory states (intact, permeabilized, complex I+II, maximal Electron Transport Chain activity) were strongly correlated with each other (correlation coefficient around 0.9), suggesting that none of the respiratory complexes underwent specific changes. Leak respiration showed somewhat lower correlations with other respiratory states (correlation coefficient 0.4-0.5), but intergroup changes were consistent across all respiratory states. Mean and median respiration values were higher in both the Fructose and STZ+lipids groups compared to the Control group. Notably, more rats in the Fructose group exhibited elevated cellular respiration, resulting in significantly higher median values compared to the Control group, especially in visceral and brown adipose tissues.

Several factors could contribute to the increased cellular respiration, including substrate availability, higher mitochondrial density, and activation of regulatory pathways. An important question is whether the additional energy is used for anabolic reactions, such as adipose tissue expansion, or dissipated as heat through uncoupled or leak respiration. We observed that in Control rats, leak respiration was much higher in brown adipose tissue (BAT) than in white adipose tissue (WAT) or SAT. In contrast, in experimental groups, leak respiration increased in VAT and SAT, reaching BAT levels. However, BAT showed consistent median values across all three groups.

Clearly, both substrate-related ATP-producing respiration and leak respiration increased in experimental groups in different adipose tissues. Consequently, we evaluated associated metabolic and hemodynamic changes in each group separately to identify related patterns. To extract a general trend, we employed Principal Component Analysis (PCA) on respiratory state values for each tissue type. As all respiratory indexes were collinear, the first PCA component explained 85-95% of the variability, which we used for correlation analysis. In the Control group, respiratory state values exhibited less variance compared to the experimental groups and displayed significant correlations or trends with hemodynamic values such as End-Diastolic Volume (EDV), stroke volume, and mean tissue blood flow in SAT and VAT. These correlations were independent of tissue respiration, suggesting that adipose tissues with better oxygen utilization had previously received greater oxygen and glucose supplementation due to their increased metabolic activity. BAT did not show any correlations with metabolic or hemodynamic features, likely due to its distinct role as a heat producer. Factors influencing BAT respiration variability were not addressed in this study.

In the Fructose group, rats received significantly more calories, mainly from the fructose solution, resulting in calorie overflow and nutrient imbalance. While the median weight in the Fructose group did not differ significantly from the Control group, it positively correlated with triglycerides and insulin concentrations. Elevated cellular respiration in BAT positively correlated with glucose levels, heart rate, and BAT weight. In SAT, it correlated with triglycerides levels and weight, while in VAT, it correlated with triglycerides levels. Heart rate showed a significant correlation with glucose levels and calorie intake. Rats with higher triglyceride levels and heart rates exhibited a marked increase in cellular respiration in adipose tissues. Interestingly, unlike in the Control group, heart function features and tissue blood flow did not correlate with cellular respiration values in the experimental groups. It is plausible that increased cellular respiration, particularly leak respiration, contributes to delayed weight gain, as evidenced by the striking differences in calorie intake and weight gain between the Fructose and Control group animals. Elevated triglyceride levels may play a major role in this phenomenon, but further research is required for clarification.

In the STZ+lipids group, we also observed increased cellular respiration, but metabolic and hemodynamic features exhibited different patterns. We initially expected the STZ+lipids model to develop significant obesity with insulin resistance and type 2 diabetes features, as reported in the

 doi:10.20944/preprints202311.0720.v1

literature [12–14]. Shortly after the STZ injection, rats in the STZ+lipids group experienced severe hyperglycemia, with a median level around 20 mmol/l. Insulin levels decreased but not significantly compared to other groups. Another metabolic disturbance included significant hyperketonemia, likely linked to hyperglycemia. After 24 weeks, severe hemodynamic impairment was evident, with decreased heart rate and ejection fraction. Higher metabolic impairment (glucose and ketone body levels) correlated with lower body weight but also higher food consumption, although weight did not correlate with food consumption. Consequently, rats with high fat intake developed severe metabolic disturbances but gained less weight. Moreover, more intense feeding was associated with higher EDV and ESV. Glucose concentration exhibited a significant negative correlation with blood pressure and heart rate and a positive correlation with stroke volume. Cellular respiration in adipose tissues lacked correlations with both metabolic and hemodynamic features. Brown adipose tissue respiration negatively correlated only with food consumption, while SAT respiration correlated solely with heart rate. In summary, rats that consumed a lipid-enriched diet and had higher food consumption exhibited greater metabolic and hemodynamic disturbances. They displayed a tendency toward higher cellular respiration, especially in BAT.

One notable difference between the STZ+lipids and fructose models were their glucose concentration dynamics. In the pure MetS model, such as the fructose model, weight gain is often not observed, although the reasons remain incompletely understood. It is possible that rodents exhibit a high level of resilience to caloric overload, or longer durations are required to achieve significant weight gain. In contrast, the STZ+lipids model mimics type 2 diabetes, and outcomes can vary widely depending on the severity of β-cell damage. In our study, rats in the STZ+lipids group developed severe hyperglycemia, which is not conducive to weight gain.

It is well-established that obesity, hyperglycemia, and insulin resistance coincide with structural and functional alterations in mitochondria, including changes in density and dynamics (fusion and fission) [15]. Multiple studies have demonstrated decreased mitochondrial respiration in adipose tissue, skeletal muscle [16–18], and heart myocytes in insulin-deficient, insulin-resistant states, and obesity-related conditions. In these conditions, there is often a reduction in mitochondrial respiration. Furthermore, an increase in fatty acid flux, as seen in prediabetic states involving obesity and hyperglycemia, can lead to elevated substrate delivery to mitochondria, promoting ROS production, mitochondrial dysfunction, and exacerbating hyperglycemia. Impairment in mitochondrial biogenesis may also contribute to the decrease in oxidative phosphorylation and mitochondrial density observed in diabetes.

On the other hand, there is evidence of increased mitochondrial function in certain forms of obesity. For instance, studies by A. Bohm et al. have demonstrated altered mitochondrial respiration in subcutaneous adipocytes of individuals with different obesity phenotypes. Adipocytes from metabolically unhealthy subjects exhibited increased basal respiration, higher proton leak, elevated ATP production, increased maximal respiration, and higher spare respiratory capacity, compared to metabolically healthy obesity. These findings were negatively correlated with the insulin sensitivity of the donors [19]. Our studies in rat adipose tissue depots support these findings, although we did not observe signs of insulin resistance in the two MetS models. We used the HOMA-IR index for insulin resistance assessment, which was originally developed for humans. Therefore, it is possible that this index may not accurately reflect insulin sensitivity in rats [20,21]. In both MetS models, we observed increased respiration in all types of adipose tissues, but the increase was associated with rats in different metabolic states. In the Fructose model, increased respiration corresponded to rats with less severe dyslipidemia, whereas in the STZ+lipids model, it was associated with rats with higher food consumption and worse glucose and ketone body levels. Therefore, the STZ+lipids model more closely resembles the metabolically unhealthy human obesity phenotype, despite not exhibiting severe obesity.

Another noteworthy finding in our study pertains to hemodynamic changes. In the Control group, better hemodynamic values correlated with higher respiration rates in adipose tissues. However, this correlation did not hold true in the experimental groups. Additionally, hemodynamics was impaired in the MetS models, despite the observed increase in respiration. Hemodynamic

 doi:10.20944/preprints202311.0720.v1

impairment in MetS and diabetes can have multiple causes. Elevated glucose levels and other agents can damage the endothelial lining of blood vessels. Patients with insulin resistance have been shown to have reduced nitric oxide synthase (NOS) expression and subsequent nitric oxide (NO) production in endothelial cells (ECs). This makes vessels more susceptible to the harmful effects of oxidized lipids and atherosclerosis development. High blood glucose stimulates prenylation of ECs' Ras and Rho proteins, enhancing their response to angiotensin II (AT II), epidermal growth factor (EGF), and platelet-derived growth factor, leading to increased growth stimulation and mitogenic response [22–24]. Additionally, cardiomyocyte contractile activity can be reduced in patients with MetS, involving changes in the expression of ryanodine receptor type 2 (RyR2) and SERCA2a, leading to abnormalities in calcium cycling during contraction [25–28].

In conclusion, our study sheds light on the intricate interplay between cellular respiration, metabolic changes, and hemodynamic alterations in different models of MetS and diabetes in rats. The findings highlight the variability in metabolic and hemodynamic responses within and between these models. It is evident that the relationship between mitochondrial respiration, metabolic disturbances, and hemodynamic changes is complex and context dependent. Further research is warranted to elucidate the precise mechanisms underlying these interactions and their implications for metabolic and cardiovascular health.

4. Materials and Methods

Animal Handling

The experiment received approval from the local bioethics committee during its 147-d meeting held on December 16, 2022. Male Wistar rats with a body weight ranging from 300 to 325g (N=31) were obtained from a standard pathogen-free (SPF) breeding facility in Pushino, Russia. Throughout the experiment, the animals were housed in a certified vivarium with a 12-hour day/night cycle and were provided with ad libitum access to food and water. Upon arrival, the animals were categorized into their respective groups based on their body weight and placed in standard T3 cages accommodating three rats each. After an initial 2-week period of acclimatization and handling, baseline biochemical and physiological assessments were conducted over a 2-week period. The experimental diet was initiated at the beginning of the experiment, and measurements were repeated after 24 weeks to assess metabolic and hemodynamic features.

A total of 31 animals were distributed into three groups: 8 in the Control group, 11 in the Fructose group, and 12 in the Streptozotocin + Lipids (STZ+lipids) group. Rats in the Control group were fed a standard chow diet (comprising 3.8% fat, 52.1% carbohydrates, 20% protein, 4.3% fiber, and 1.3% salt based on wet weight) and had free access to tap water. In the Fructose group, water was replaced with a 20% fructose solution, while the STZ+lipids group received a micronutrient-balanced chow containing 58% of calories derived from lipids, which was achieved by mixing standard chow powder with lard, casein, and salts. Two weeks after the experiment's commencement, rats in the STZ+lipids group received an intraperitoneal injection of 25 mg/kg streptozotocin (Sigma) dissolved in 1 ml of cold citrate buffer (+4^{o}C, pH=4.5). It's noteworthy that all rats in this group developed hyperglycemia three days after the injection and remained part of the study. Mortality was not assessed in the study, as only one rat from the Control group died due to anesthesia overdose.

Rat body weight was measured using a laboratory scale (Sartorius) with a readability of 100 mg. Food and water (or fructose solution) consumption were monitored in individual cages. Food was weighed initially and after 24 hours, including any visible remnants within the cage. Similarly, water weight was recorded in the bottle before and after 24-hour caging. Total caloric intake, nutrient and pure water consumption were calculated based on these values.

Biochemical Analysis

Blood glucose and ketone body concentrations were assessed in mixed blood samples obtained from tail tips using a glucometer (One Touch Verio Pro) and a ketone bodies analyzer (Optium Xceed), both equipped with original test strips. The samples were collected from conscious rats using a sterile scarificator. A volume of 2 ml of blood was drawn from the jugular vein under isoflurane

 doi:10.20944/preprints202311.0720.v1

anesthesia, with citrate anticoagulant added. The blood was then centrifuged at 1000g for 10 minutes in a refrigerated centrifuge (Eppendorf 5804R), and the plasma layer was collected. Subsequently, insulin, glucose, and triglyceride concentrations were measured in the plasma samples. Glucose and triglyceride concentrations were determined using standard colorimetric kits (Vector-Best, Russia), while insulin concentration was measured using ELISA kits (Vektor-Best, Russia), following the manufacturer's protocol. Colorimetric and ELISA assays were performed at 37°C using a PerkinElmer Enspire plate reader at the appropriate wavelengths. All measurements were conducted in triplicate, and concentrations were calculated from calibration curves constructed using kit control samples.

Physiological Tests

Blood pressure and heart rate were recorded in conscious rats using a tail cuff and photoplethysmography (Systola, Neurobiotics, Russia). The rat's tail was preheated for 15 minutes, and the rats were placed in immobilizers on heated pads. Arterial pressure was recorded over a 15-minute duration.

Rats were exposed to isoflurane (Karizoo, Spain) for ultrasound and echocardiographic evaluations. Unconscious rats were securely positioned on a heated rotating operating table, and specific areas, including the chest, abdominal wall, left inguinal region, and inter-scapular region, were shaved. All ultrasound and echocardiography studies were conducted using a Mindray M5 New (Mindray, China) apparatus equipped with a 12 mHz linear transducer. Measurements included the thickness of the subcutaneous inguinal fat pad in relation to the femoral joint, the maximal area of the left brown fat pad, and the maximal horizontal area of the pararenal visceral fat. Cardiac assessments were performed in both long-axis and short-axis parasternal positions, and parameters such as end-systolic volume, end-diastolic volume, stroke volume, and ejection fraction were calculated based on these measurements. Mean tissue blood flow was measured using a laser-Doppler device (BLF21D, Transonic Devices) with a thin probe. Signal processing was carried out using a Biopac MP35 ADC and analyzed with BSL Pro software. The probe was placed on the interscapular back skin using a damping holder, and mean blood flow values were calculated from a 1-minute recording.

Respirometry Study

After 24 weeks of the experiment, animals were euthanized through a stepwise overdose of chloral hydrate. Brown fat pads were weighed using a Sartorius balance with a readability of 10 mg, and adipose tissue samples were analyzed in the following order: brown fat sample (approximately 20 mg), visceral fat sample (approximately 50 mg from the abdominal cavity), and inguinal subcutaneous fat sample (approximately 30 mg). Tissue samples were precisely weighed using an analytical scale (Ohaus AX224) before the respirometry assays and placed in cold respiration buffer.

All oxygen consumption rate (OCR) tests were conducted using the Oxygraph module (HansaTech instruments) with a standard liquid chamber and Oxygraph software. The oxygen sensor was calibrated at the beginning of each experimental day using an internal program with sodium dithionite. Prior to the tests, tissue samples were immersed in 1 ml of Mir05 respiration buffer medium (composed of 110 mM sucrose, 60 mM potassium lactobionate, 20 mM HEPES, 10 mM KH_2PO_4, 3 mM $MgCl_2$, 0.5 mM EGTA, pH 7.4, reagents from Sigma) at a room temperature. The chamber and plunger were rinsed multiple times with ultrapure water between different runs. Tissue samples were kept in the cold solution for up to 10 minutes before the study. A simplified SUIT (substrate-uncoupler-inhibitor titration protocol) respiration protocol was used to conduct multiple tissue tests sequentially within one Oxygraph chamber. Each substrate and inhibitor were added only once to achieve maximum effect in a short duration, based on preliminary research on liver samples. The next step was initiated after the OCR had stabilized. Short steps were also feasible due to the relatively large size of the tissue samples, allowing for rapid absorption of inhibitors. On average, each tissue test run lasted about 10 minutes.

The following sequence of steps was employed during the respirometry assays:

1. **Intact Respiration**: Tissue samples were initially placed in the chamber to measure intact respiration.

 doi:10.20944/preprints202311.0720.v1

2. **Permeabilized Base Respiration (State 2)**: 5 mg/ml saponin (Macklin, China) was taken for tissue permeabilization, 5 mM sodium malate and 5 mM sodium pyruvate (Sigma) were added to stimulate permeabilized base respiration (State 2).
3. **Stimulation of State 3 Respiration Through Complex I**: 2 mM ADP (magnesium stabilized, Sigma) was added to stimulate state 3 respiration through complex I.
4. **Maximal Respiration Through Complexes I and II**: 5 mM sodium succinate (Sigma) was added to achieve maximal respiration through complexes I and II.
5. **State 4 Respiration (Leak)**: State 4 respiration (leak) was measured after injecting 10 nM oligomycin (Sigma).
6. **Maximal Respiratory Capacity (Uncoupled Respiration)**: Maximal respiratory capacity (uncoupled respiration) was measured after adding 1 mM carbonyl cyanide m-chlorophenyl hydrazone (CCCP, Sigma) in DMSO (Sigma).
7. **Complex I-Specific Respiration Rate**: Following OCR stabilization, rotenone (Sigma) was added to measure complex I-specific respiration rate.
8. **Residual (Background) Respiration**: Finally, 5 mM antimycin A (Sigma) was added to measure residual (background) respiration.

Raw oxygen concentration data were recorded and saved in .csv format for further analysis.

Data Processing and Statistical Analysis

All data processing and analysis were conducted using the Python 3.8 programming language and open-source code libraries. The Pandas and Numpy libraries were utilized for converting raw data into tables and processing oxygen concentrations into OCR using a consistent algorithm. The table of oxygen concentrations was segmented based on reagent addition events, and 10-second margins were trimmed to eliminate external O_2 fluctuations. Within each segment between two events, the median oxygen shift over 1 second was calculated to reduce noise. The averaged median shifts within the segment were then used to calculate raw OCR. Weight-adjusted values were computed to obtain measurements in nmol/s/ml/g dimensions. All values were corrected for residual respiration rate and converted to absolute values. The resulting data were utilized for subsequent statistical analyses.

Statistical analyses were performed using the Statsmodels and Scipy libraries. Due to the relatively small sample sizes, non-parametric statistical tests and universal statistical models were employed. The Statsmodels library's mixed-effects generalized linear model (GLM) was used to analyze time-dependent changes. For dependent variables, the Kruskal-Wallis test was employed, followed by post-hoc multiple comparisons using the Dwass-Steel-Critchlow-Fligner (DSCF) test. Screening correlation analyses were conducted using simple Pearson R calculations and heatmaps. Dimensionality reduction of respiration states was achieved through primary component analysis using Scikit-learn functions to identify general correlations. All p-values less than 0.05 were considered statistically significant. Data visualization was carried out using boxplots, depicting medians, quartiles, and minimum/maximum values, with Matplotlib and Seaborn libraries facilitating plot creation.

Supplementary Materials: The following supporting information can be downloaded at the website of this paper posted on Preprints.org., Figure S1: Correlation heatmap, metabolic features; Figure S2: Correlation heatmap, hemodynamic features; Table S3: Raw data.

Author Contributions: Conceptualization: E.I., S.G.; methodology, E.I.; software, A.E.; validation: A.E., M.A., S.G.; formal analysis: E.I.; investigation: E.I., A.R.; resources; E.I., A.E., M.A., A.R., S.G.; data curation, E.I., A.E.; writing, original draft preparation, E.I., writing, review, and editing: E.I., A.E., M.A., A.R., S.G.; visualization, E.I., S.G.; supervision, S.G.; project administration, E.I. All authors have read and agreed to the published version of the manuscript.

Funding: Research was funded by Russian Science Foundation grant № 22-25-00344, https://rscf.ru/project/22-25-00344/.

Institutional Review Board Statement: "The animal study protocol was approved by the Institutional Ethics Committee of Moscow State University (protocol code 147-d date of approval 16.12.2022)."

Data Availability Statement: Raw data presented in supplementary material 3.

Conflicts of Interest: The authors declare no conflicts of interest.

References

1. Purwowiyoto, S.L.; Prawara, A.S. Metabolic Syndrome and Heart Failure: Mechanism and Management. *Med Pharm Rep* **2021**, *94*, 15–21, doi:10.15386/MPR-1884.
2. Hoetama, E.; Hermawan, B. Metabolic Syndrome : An Emerging Risk Factor for Congestive Heart Failure. *Indonesian Journal of Cardiology* **2015**, *36*, 145–150, doi:10.30701/IJC.V36I3.477.
3. Perrone-Filardi, P.; Paolillo, S.; Costanzo, P.; Savarese, G.; Trimarco, B.; Bonow, R.O. The Role of Metabolic Syndrome in Heart Failure. *Eur Heart J* **2015**, *36*, 2630–2634, doi:10.1093/EURHEARTJ/EHV350.
4. Wilson, P.W.F.; D'Agostino, R.B.; Parise, H.; Sullivan, L.; Meigs, J.B. Metabolic Syndrome as a Precursor of Cardiovascular Disease and Type 2 Diabetes Mellitus. *Circulation* **2005**, *112*, 3066–3072, doi:10.1161/CIRCULATIONAHA.105.539528.
5. Rajab, B.S.; Kassab, S.; Stonall, C.D.; Daghistani, H.; Gibbons, S.; Mamas, M.; Smith, D.; Mironov, A.; AlBalawi, Z.; Zhang, Y.H.; et al. Differential Remodelling of Mitochondrial Subpopulations and Mitochondrial Dysfunction Are a Feature of Early Stage Diabetes. *Sci Rep* **2022**, *12*, doi:10.1038/S41598-022-04929-1.
6. Gancheva, S.; Kahl, S.; Pesta, D.; Mastrototaro, L.; Dewidar, B.; Strassburger, K.; Sabah, E.; Esposito, I.; Weiß, J.; Sarabhai, T.; et al. Impaired Hepatic Mitochondrial Capacity in Nonalcoholic Steatohepatitis Associated With Type 2 Diabetes. *Diabetes Care* **2022**, doi:10.2337/DC21-1758.
7. Zhao, Q.Y.; Ge, L.H.; Zhang, K.; Chen, H.F.; Zhan, X.X.; Yang, Y.; Dang, Q.L.; Zheng, Y.; Zhou, H. Bin; Lyu, J.X.; et al. Assessment of Mitochondrial Function in Metabolic Dysfunction-Associated Fatty Liver Disease Using Obese Mouse Models. *Zool Res* **2020**, *41*, 539, doi:10.24272/J.ISSN.2095-8137.2020.051.
8. Boardman, N.T.; Pedersen, T.M.; Rossvoll, L.; Hafstad, A.D.; Aasum, E. Diet-Induced Obese Mouse Hearts Tolerate an Acute High-Fatty Acid Exposure That Also Increases Ischemic Tolerance. *Am J Physiol Heart Circ Physiol* **2020**, *319*, H682–H693, doi:10.1152/AJPHEART.00284.2020.
9. Mancuso, D.J.; Sims, H.F.; Yang, K.; Kiebish, M.A.; Su, X.; Jenkins, C.M.; Guan, S.; Moon, S.H.; Pietka, T.; Nassir, F.; et al. Genetic Ablation of Calcium-Independent Phospholipase A2γ Prevents Obesity and Insulin Resistance during High Fat Feeding by Mitochondrial Uncoupling and Increased Adipocyte Fatty Acid Oxidation. *J Biol Chem* **2010**, *285*, 36495, doi:10.1074/JBC.M110.115766.
10. Beaudoin, M.S.; Snook, L.A.; Arkell, A.M.; Simpson, J.A.; Holloway, G.P.; Wright, D.C. Resveratrol Supplementation Improves White Adipose Tissue Function in a Depot-Specific Manner in Zucker Diabetic Fatty Rats. *Am J Physiol Regul Integr Comp Physiol* **2013**, *305*, 542–551, doi:10.1152/AJPREGU.00200.2013/ASSET/IMAGES/LARGE/ZH60171382730006.JPEG.
11. Pesta, D.; Gnaiger, E. High-Resolution Respirometry: OXPHOS Protocols for Human Cells and Permeabilized Fibers from Small Biopsies of Human Muscle. *Methods in Molecular Biology* **2012**, *810*, 25–58, doi:10.1007/978-1-61779-382-0_3/FIGURES/9_3.
12. Al-Awar, A.; Kupai, K.; Veszelka, M.; Szűcs, G.; Attieh, Z.; Murlasits, Z.; Török, S.; Pósa, A.; Varga, C. Experimental Diabetes Mellitus in Different Animal Models. *J Diabetes Res* **2016**, *2016*, 9051426, doi:10.1155/2016/9051426.
13. Sah, S.P.; Singh, B.; Choudhary, S.; Kumar, A. Animal Models of Insulin Resistance: A Review. *Pharmacological Reports* **2016**, *68*, 1165–1177, doi:10.1016/j.pharep.2016.07.010.
14. Aleixandre de Artiñano, A.; Miguel Castro, M. Experimental Rat Models to Study the Metabolic Syndrome. *British Journal of Nutrition* **2009**, *102*, 1246, doi:10.1017/S0007114509990729.
15. Li, J.; Li, J.; Chen, Y.; Hu, W.; Gong, X.; Qiu, H.; Chen, H.; Xin, Y.; Li, H. The Role of Mitochondria in Metabolic Syndrome-Associated Cardiomyopathy. *Oxid Med Cell Longev* **2022**, *2022*, doi:10.1155/2022/9196232.
16. Sivitz, W.I. Mitochondrial Dysfunction in Obesity and Diabetes. *US Endocrinol* **2010**, *6*, 20–27, doi:10.17925/USE.2010.06.1.20.
17. Boudina, S.; Sena, S.; Theobald, H.; Sheng, X.; Wright, J.J.; Xia, X.H.; Aziz, S.; Johnson, J.I.; Bugger, H.; Zaha, V.G.; et al. Mitochondrial Energetics in the Heart in Obesity-Related Diabetes: Direct Evidence for Increased Uncoupled Respiration and Activation of Uncoupling Proteins. *Diabetes* **2007**, *56*, 2457–2466, doi:10.2337/DB07-0481.
18. Mogensen, M.; Sahlin, K.; Fernström, M.; Glintborg, D.; Vind, B.F.; Beck-Nielsen, H.; Højlund, K. Mitochondrial Respiration Is Decreased in Skeletal Muscle of Patients with Type 2 Diabetes. *Diabetes* **2007**, *56*, 1592–1599, doi:10.2337/DB06-0981.
19. Böhm, A.; Keuper, M.; Meile, T.; Zdichavsky, M.; Fritsche, A.; Häring, H.U.; de Angelis, M.H.; Staiger, H.; Franko, A. Increased Mitochondrial Respiration of Adipocytes from Metabolically Unhealthy Obese

Compared to Healthy Obese Individuals. *Scientific Reports 2020 10:1* **2020**, *10*, 1–10, doi:10.1038/s41598-020-69016-9.

20. Wei, M.; Zhan, D.; Li, Z.X.; Wang, H.Y.; Xing, Y.; Luo, X.P. Effect of High-Fat Diet for Rats at Different Stages on Glucose and Lipid Metabolism in Offspring and Related Mechanisms. *Zhongguo Dang Dai Er Ke Za Zhi* **2021**, *23*, 1174–1183, doi:10.7499/J.ISSN.1008-8830.2107121.
21. Antunes, L.C.; Elkfury, J.L.; Jornada, M.N.; Foletto, K.C.; Bertoluci, M.C. Validation of HOMA-IR in a Model of Insulin-Resistance Induced by a High-Fat Diet in Wistar Rats. *Arch Endocrinol Metab* **2016**, *60*, 138–142, doi:10.1590/2359-3997000000169.
22. Zhou, M.S.; Wang, A.; Yu, H. Link between Insulin Resistance and Hypertension: What Is the Evidence from Evolutionary Biology? *Diabetol Metab Syndr* **2014**, *6*, doi:10.1186/1758-5996-6-12.
23. Schulman, I.H.; Zhou, M.S. Vascular Insulin Resistance: A Potential Link between Cardiovascular and Metabolic Diseases. *Curr Hypertens Rep* **2009**, *11*, 48–55, doi:10.1007/S11906-009-0010-0.
24. Zafar, U.; Khaliq, S.; Ahmad, H.U.; Manzoor, S.; Lone, K.P. Metabolic Syndrome: An Update on Diagnostic Criteria, Pathogenesis, and Genetic Links. *Hormones 2018 17:3* **2018**, *17*, 299–313, doi:10.1007/S42000-018-0051-3.
25. Lavorato, M.; Huang, T.Q.; Iyer, V.R.; Perni, S.; Meissner, G.; Franzini-Armstrong, C. Dyad Content Is Reduced in Cardiac Myocytes of Mice with Impaired Calmodulin Regulation of RyR2. *J Muscle Res Cell Motil* **2015**, *36*, 205–214, doi:10.1007/S10974-015-9405-5.
26. Santulli, G.; Pagano, G.; Sardu, C.; Xie, W.; Reiken, S.; D'Ascia, S.L.; Cannone, M.; Marziliano, N.; Trimarco, B.; Guise, T.A.; et al. Calcium Release Channel RyR2 Regulates Insulin Release and Glucose Homeostasis. *J Clin Invest* **2015**, *125*, 1968–1978, doi:10.1172/JCI79273.
27. Okatan, E.N.; Durak, A.T.; Turan, B. Electrophysiological Basis of Metabolic-Syndrome-Induced Cardiac Dysfunction. *Can J Physiol Pharmacol* **2016**, *94*, 1064–1073, doi:10.1139/CJPP-2015-0531.
28. Deniz Dincer, U. Cardiac Ryanodine Receptor in Metabolic Syndrome: Is JTV519 (K201) Future Therapy? *Diabetes Metab Syndr Obes* **2012**, *5*, 89–99, doi:10.2147/DMSO.S30005.